

# Structural and Optical Properties of Hydrothermally Synthesized ZnO and Zn<sub>0.99</sub>O:Eu<sup>3+</sup> Powders

K. PARK<sup>a,\*</sup>, D.A. HAKEEM<sup>a</sup>, J. KIM<sup>b</sup>, Y. KIM<sup>c</sup> AND S.-J. KIM<sup>d</sup>

<sup>a</sup>Faculty of Nanotechnology and Advanced Materials Engineering, Sejong University, Seoul 143-747, Korea

<sup>b</sup>Department of Advanced Materials Engineering, Hoseo University, Asan 336-795, Korea

<sup>c</sup>Department of Chemistry, Dankook University, Cheonan, Chungnam 330-714, Korea

<sup>d</sup>Department of Advanced Materials and Chemical Engineering, Halla University, Wonju, Kangwon 220-712, Korea

The structural and optical properties of the ZnO and Zn<sub>0.99</sub>O:Eu<sup>3+</sup> powders synthesized by the hydrothermal method at two different temperatures (150 °C and 250 °C) were studied. The ZnO and Zn<sub>0.99</sub>O:0.01Eu<sup>3+</sup> powders synthesized at 150 and 250 °C showed rod- and flower-like morphologies, respectively. The as-synthesized and annealed ZnO and Zn<sub>0.99</sub>O:0.01Eu<sup>3+</sup> powders formed the wurtzite crystal structure and *P6<sub>3</sub>mc* space group. The crystallite size of the as-synthesized and annealed ZnO powders increased by the incorporation of Eu<sup>3+</sup>. The photoluminescence properties of annealed Zn<sub>0.99</sub>O:0.01Eu<sup>3+</sup> powders were substantially improved by controlling the synthesis temperature. The annealed Zn<sub>0.99</sub>O:0.01Eu<sup>3+</sup> powders synthesized at 250 °C displayed much stronger emission intensity than those at 150 °C.

DOI: [10.12693/APhysPolA.133.902](https://doi.org/10.12693/APhysPolA.133.902)

PACS/topics: 78.55.-m, 78.55.Hx, 78.55.Et

## 1. Introduction

White light emitting diodes (LEDs) emerge as a vital alternative to replace traditional incandescent and fluorescent lighting because of their high energy saving, high efficiency, long lifetime, and environmentally friendly characteristics [1, 2]. The white light can be achieved by three different ways, namely, (1) red (R), green (G), and blue (B) LED chips, (2) the combination of a blue LED chip and yellow phosphor, and (3) the combination of a blue/ultraviolet (UV) LED chip and RGB phosphors [3, 4]. Among these ways, white lighting by means of RGB phosphors is highly promising owing to the following advantages: high photoluminescence (PL) efficiency, a high color rendering index (CRI), and a tunable correlated color temperature (CCT). It is known that the PL efficiency, CRI, and CCT of white LEDs depend strongly on the performance of the phosphors used [5]. Therefore, significant attention has been paid on the development of rare earth ions-doped phosphors. Y<sub>2</sub>O<sub>2</sub>S:Eu<sup>3+</sup> is a commonly used red-emitting phosphor. However, the phosphor exhibits lower emission efficiency in comparison with blue and green phosphors, evolution of harmful gas such as sulphide, and insufficient absorption in the near-UV/blue region [6, 7]. It is thus necessary to develop efficient red-emitting phosphors with high stability and absorption efficiency in the near-UV/blue region for white LED applications.

Zinc oxide (ZnO) is an inorganic II–VI group semiconductor with a wide band gap (3.3 eV), high exciton binding energy (60 meV), high transparency, high

electron mobility, and strong room-temperature luminescence [8, 9]. The wide band gap provides high breakdown voltage (75 V), high ability to sustain large electric fields, low electronic noise, and high power operation. In addition, the high exciton binding energy offers high stability against thermal dissociation of excitons, which is necessary for optoelectronic devices [9]. These unique properties have made ZnO to be a very attractive material for the applications of LEDs, scintillators, sensors, and solar cells [8, 10]. In addition, ZnO has been used as a host material for doping rare earth metal ions and/or transition metal ions to emit blue, green, or red light; the doping can modify the electronic structure of ZnO, improving significantly its PL properties.

It has been known that controlling the composition and synthesis process is a feasible route for improving PL performance. In this work, the structural and optical properties of the ZnO and Eu<sup>3+</sup>-doped Zn<sub>0.99</sub>O:0.01Eu<sup>3+</sup> phosphors were studied. We doped 0.01Eu<sup>3+</sup> into ZnO because the solubility limit of Eu<sub>2</sub>O<sub>3</sub> in ZnO is approximately 2 mol.% [11–13]. The secondary phases related to Eu<sub>2</sub>O<sub>3</sub> can be formed above this solubility. The ZnO and Zn<sub>0.99</sub>O:0.01Eu<sup>3+</sup> phosphors were synthesized by the hydrothermal method at two different temperatures (150 and 250 °C) by using Zn(NO<sub>3</sub>)<sub>2</sub>, Eu(NO<sub>3</sub>)<sub>3</sub>, and KOH. The hydrothermal synthesis method is an attractive technique with several benefits, such as effective control of size, morphology, and agglomeration of the particles, a relatively low reaction temperature, cost effectiveness, and environmentally benign route [14].

## 2. Experimental

The hydrothermal method was used for synthesizing ZnO and Zn<sub>0.99</sub>O:0.01Eu<sup>3+</sup> powders. Eu<sub>2</sub>O<sub>3</sub> was dissolved in HNO<sub>3</sub> and heated to prepare Eu(NO<sub>3</sub>)<sub>3</sub>.

\*corresponding author; e-mail: [kspark@sejong.ac.kr](mailto:kspark@sejong.ac.kr)

Zn(NO<sub>3</sub>)<sub>2</sub>, Eu(NO<sub>3</sub>)<sub>3</sub>, and KOH were separately dissolved in deionized water and then mixed together. The resultant mixture was stirred for 1 h with a magnetic stirrer to prepare a homogeneous solution. The solution was transferred into a teflon-lined stainless steel autoclave with a capacity of 300 ml, heated at two different temperatures (150 and 250 °C) for 6 h, and then naturally cooled down to room temperature. The resultant powders were separated from the solution by centrifugation, washed with ethanol and distilled water several times, and dried at 60 °C for 24 h in an oven. Finally, the as-synthesized powders were cooled down slowly to room temperature and then ground into powders. The size and morphological characteristics of the as-synthesized ZnO and Zn<sub>0.99</sub>O:0.01Eu<sup>3+</sup> powders were investigated with a field-emission scanning electron microscope (FE-SEM; Hitachi S4700, Japan). The binding energy of constituent elements in the as-synthesized ZnO and Zn<sub>0.99</sub>O:0.01Eu<sup>3+</sup> powders was investigated by X-ray photoelectron spectroscopy (XPS; K<sub>α</sub>, Thermo VG, U.K.). The crystal structure of as-synthesized and annealed ZnO and Zn<sub>0.99</sub>O:0.01Eu<sup>3+</sup> powders was analyzed with an X-ray diffractometer (XRD; Rigaku RINT2000, Japan). The PL spectra of the powders were obtained with a spectrofluorometer (FS-2, Scinco Co., Korea) equipped with a xenon lamp. All emission spectra were obtained using the same amount of phosphors and recorded under the same conditions.

### 3. Results and discussion

FE-SEM images of the ZnO and Zn<sub>0.99</sub>O:0.01Eu<sup>3+</sup> powders synthesized at 150 and 250 °C are shown in Fig. 1. The morphology of the ZnO and Zn<sub>0.99</sub>O:0.01Eu<sup>3+</sup> powders depends strongly on the synthesis temperature. The ZnO and Zn<sub>0.99</sub>O:0.01Eu<sup>3+</sup> powders synthesized at 150 °C show a rod-like morphology (300–600 nm in length and 150–250 nm in diameter), and its powder sizes increase by doping Eu<sup>3+</sup> into the ZnO. On the other hand, the ZnO and Zn<sub>0.99</sub>O:0.01Eu<sup>3+</sup> powders synthesized at 250 °C show a flower-like morphology. A similar behavior was reported for the NaLa(MoO<sub>4</sub>)<sub>2</sub> powders prepared by the hydrothermal method [15].

Figure 2a displays the XPS survey spectra of the ZnO and Zn<sub>0.99</sub>O:0.01Eu<sup>3+</sup> powders synthesized at 250 °C. The XPS survey spectra show the peaks corresponding to the constituent elements, Zn, Eu, and O. The high-resolution spectra of Zn 2*p* and O 1*s* for the ZnO and Zn<sub>0.99</sub>O:0.01Eu<sup>3+</sup> powders synthesized at 250 °C are presented in Fig. 2b and c, respectively, and that of Eu 3*d* for the Zn<sub>0.99</sub>O:0.01Eu<sup>3+</sup> powders is presented in Fig. 2d. The high-resolution spectra of Zn in ZnO powders exhibit two peaks at 1021.5 and 1044.5 eV, which are attributed to the Zn 2*p*<sub>3/2</sub> and Zn 2*p*<sub>1/2</sub>, respectively (Fig. 2b). This suggests that Zn ions exist in a divalent-oxidation state. Similarly, the Zn 2*p*<sub>3/2</sub> and Zn 2*p*<sub>1/2</sub> peaks in Zn<sub>0.99</sub>O:0.01Eu<sup>3+</sup> powders are located at 1022.0 and 1045.0 eV, respectively. The binding energies of the

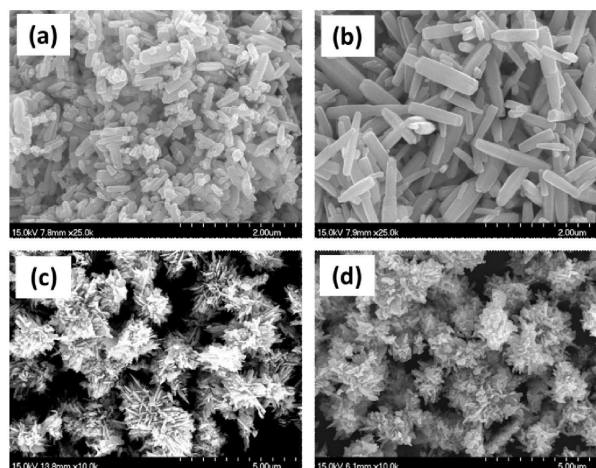


Fig. 1. FE-SEM images of the (a) ZnO and (b) Zn<sub>0.99</sub>O:0.01Eu<sup>3+</sup> powders synthesized at 150 °C and of the (c) ZnO and (d) Zn<sub>0.99</sub>O:0.01Eu<sup>3+</sup> powders synthesized at 250 °C.

Zn 2*p* peaks for the Zn<sub>0.99</sub>O:0.01Eu<sup>3+</sup> powders are 0.5 eV larger than those of ZnO powders. The higher binding energies are caused by the electronic interaction between the ZnO and Eu<sup>3+</sup> [16]. The high-resolution spectra of O 1*s* for the ZnO and Zn<sub>0.99</sub>O:0.01Eu<sup>3+</sup> powders are presented in Fig. 2c. The peaks are slightly shifted toward the higher binding energy with the incorporation of Eu<sup>3+</sup>. The binding energies of ZnO powders are 530.4 and 532.2 eV, and those of Zn<sub>0.99</sub>O:0.01Eu<sup>3+</sup> powders are 531.0 and 532.5 eV, indicating the presence of two kinds of oxygen species. The peaks at 530.4 and 531.0 eV correspond to the crystal lattice oxygen (O<sup>2-</sup>), and those at 532.2 and 532.5 eV correspond to the chemisorbed oxygen (hydroxyl species) [17]. In addition, the two intense XPS peaks related to the Eu 3*d* are detected at 1165.0 eV (Eu 3*d*<sub>3/2</sub>) and 1135.5 eV (Eu 3*d*<sub>5/2</sub>) for the Zn<sub>0.99</sub>O:0.01Eu<sup>3+</sup> powders (Fig. 2d). The energy difference between the two Eu<sup>3+</sup> peaks is found to be 29.5 eV, which is a characteristic of a charge transfer from O 2*p* to Eu 4*f* [18]. The peaks at 1155.2 and 1125.1 eV are characteristic peaks of divalent Eu<sup>2+</sup> and a weak peak at 1143.5 corresponds to multiplet.

The XRD patterns of the ZnO and Zn<sub>0.99</sub>O:0.01Eu<sup>3+</sup> powders synthesized at 150 °C followed by annealing at 800 °C are shown in Fig. 3. All the XRD patterns are well matched with the JCPDS card No. 36-1451, corresponding to the wurtzite crystal structure and *P6<sub>3</sub>mc* space group [9]. In the wurtzite crystal structure of ZnO, Zn atoms occupy at (1/3, 2/3, 0) and (2/3, 1/3, 1/2) sites, and O atoms occupy half of tetrahedrally coordinated sites at (1/3, 2/3, 3/8) and (2/3, 1/3, 7/8). The atomic arrangement of Zn and O results in non-centrosymmetric crystal and the ZnO consists of alternating layers of tetrahedrally co-ordinated O<sup>2-</sup> and Zn<sup>2+</sup> ions along the *c*-axis [19]. No significant difference in

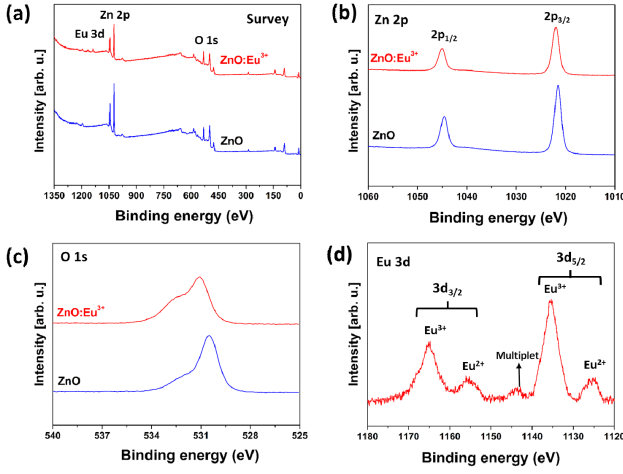


Fig. 2. XPS spectra of the ZnO and  $\text{Zn}_{0.99}\text{O}:0.01\text{Eu}^{3+}$  powders synthesized at  $250^\circ\text{C}$ : (a) survey, (b) Zn 2p, (c) O 1s, and (d) Eu 3d.

the XRD patterns of as-synthesized and annealed ZnO and  $\text{Zn}_{0.99}\text{O}:0.01\text{Eu}^{3+}$  powders is observed, indicating that both the annealing and the incorporation of  $\text{Eu}_2\text{O}_3$  do not affect the crystal structure of the ZnO. In addition, the XRD patterns of the ZnO and  $\text{Zn}_{0.99}\text{O}:0.01\text{Eu}^{3+}$  powders synthesized at  $250^\circ\text{C}$  are quite similar to those of the powders at  $150^\circ\text{C}$ , as shown in Fig. 4. The crystallite sizes ( $D$ ) of the as-synthesized and annealed ZnO and  $\text{Zn}_{0.99}\text{O}:0.01\text{Eu}^{3+}$  powders are calculated by using the Scherrer formula [20]:  $D = (0.9\lambda)/(\beta\cos\theta)$ , where  $\lambda$  is the wavelength of radiation,  $\theta$  is the angle of the diffraction peak, and  $\beta$  is the full width at half maximum of the diffraction peak (in rad). The calculated crystallite sizes of the powders are given in Table I. The crystallite sizes of annealed ZnO and  $\text{Zn}_{0.99}\text{O}:0.01\text{Eu}^{3+}$  powders are larger than those of as-synthesized powders, and those of as-synthesized and annealed  $\text{Zn}_{0.99}\text{O}:0.01\text{Eu}^{3+}$  powders are larger than those of as-synthesized and annealed ZnO powders.

TABLE I

Crystallite sizes [nm] of the as-synthesized and annealed ZnO and  $\text{Zn}_{0.99}\text{O}:0.01\text{Eu}^{3+}$  powders

Synthesis temperature [ $^\circ\text{C}$ ]	As-synthesized		Annealed	
	ZnO	$\text{ZnO}:0.01\text{Eu}^{3+}$	ZnO	$\text{ZnO}:0.01\text{Eu}^{3+}$
150	38.4	41.3	42.0	42.6
250	32.2	32.6	41.5	42.1

Figure 5 shows the excitation spectra, monitored at a wavelength of 614 nm, for the annealed ZnO and  $\text{Zn}_{0.99}\text{O}:0.01\text{Eu}^{3+}$  powders synthesized at 150 and  $250^\circ\text{C}$ . The broad excitation band centered at 378 nm may be due to the crystal defects, e.g., single-ionized oxygen vacancies, of the ZnO [21]. In addition, the sharp peaks are observed at 396, 418, 465, and 535 nm,

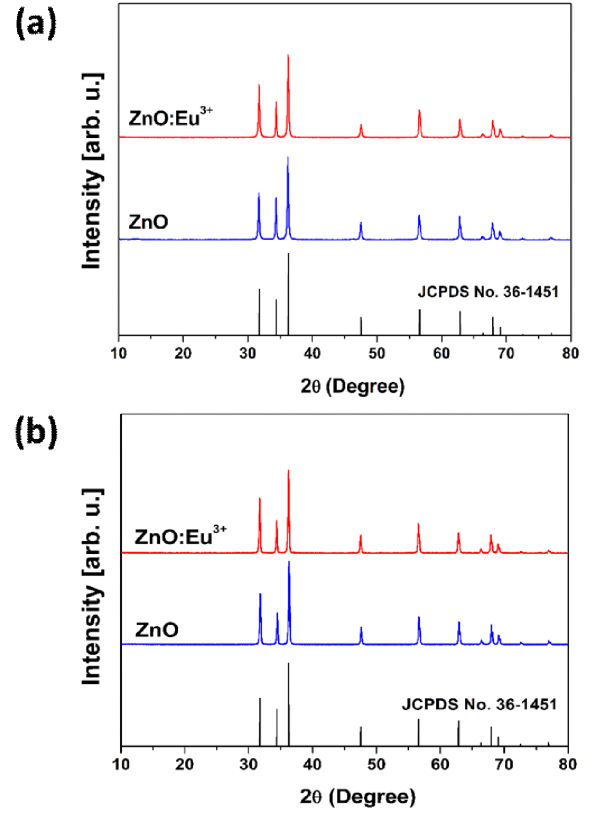


Fig. 3. XRD patterns of the (a) ZnO and  $\text{Zn}_{0.99}\text{O}:0.01\text{Eu}^{3+}$  powders synthesized at  $150^\circ\text{C}$  and of the annealed (b) ZnO and  $\text{Zn}_{0.99}\text{O}:0.01\text{Eu}^{3+}$  powders synthesized at  $150^\circ\text{C}$ .

which are attributed to the  ${}^7F_0 \rightarrow {}^5L_6$ ,  ${}^7F_0 \rightarrow {}^5D_3$ ,  ${}^7F_0 \rightarrow {}^5D_2$ , and  ${}^7F_0 \rightarrow {}^5D_1$  transitions of  $\text{Eu}^{3+}$  ions, respectively [22]. The intensity of the excitation peak at 465 nm for the annealed  $\text{Zn}_{0.99}\text{O}:0.01\text{Eu}^{3+}$  powders synthesized at  $250^\circ\text{C}$  is much stronger than that at  $150^\circ\text{C}$ . It is thus necessary to control the synthesis temperature of  $\text{Zn}_{0.99}\text{O}:0.01\text{Eu}^{3+}$  powders for increase of the excitation intensity.

The emission spectra of the annealed  $\text{Zn}_{0.99}\text{O}:0.01\text{Eu}^{3+}$  powders synthesized at 150 and  $250^\circ\text{C}$  upon 465 nm excitation are shown in Fig. 6. The broad emission band below 575 nm, corresponding to green emission, is attributed to the recombination luminescence of single-ionized oxygen vacancies [23]. Strong emission peaks are detected at 580, 592, 612, 653, and 705 nm, which originate from the transition of  $\text{Eu}^{3+}$  ions from the  ${}^5D_0$  excited state to the  ${}^7F_J$  ( $J = 0, 1, 2, 3,$  and  $4$ ) ground state, respectively [24, 25]. It is observed that the emission peak at 612 nm ( ${}^5D_0 \rightarrow {}^7F_2$ ), corresponding to the red emission, is much stronger than that at 592 nm ( ${}^5D_0 \rightarrow {}^7F_1$ ), corresponding to orange emission. This suggests that the  $\text{Eu}^{3+}$  ions are located at a non-centrosymmetric environment in ZnO lattice. Clearly, the emission intensity of the annealed

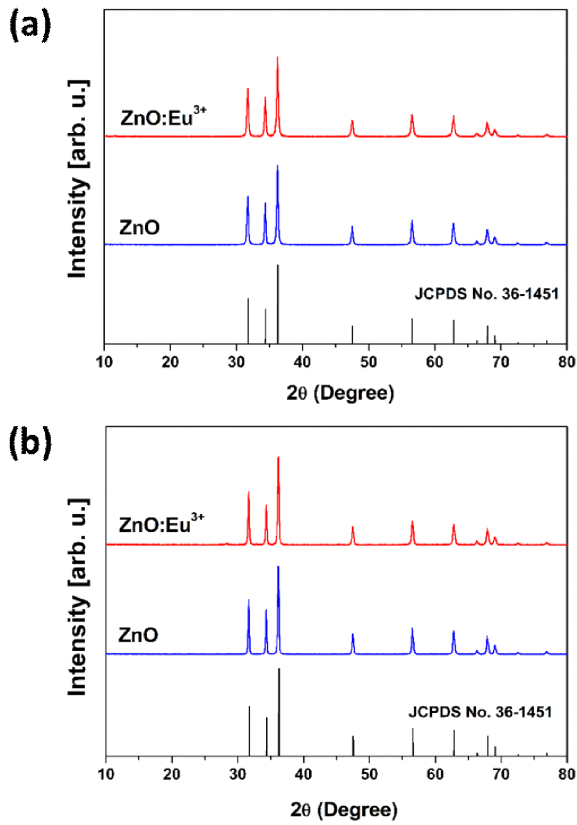


Fig. 4. XRD patterns of the (a) ZnO and  $\text{Zn}_{0.99}\text{O}:0.01\text{Eu}^{3+}$  powders synthesized at  $250^\circ\text{C}$  and of the annealed (b) ZnO and  $\text{Zn}_{0.99}\text{O}:0.01\text{Eu}^{3+}$  powders synthesized at  $250^\circ\text{C}$ .

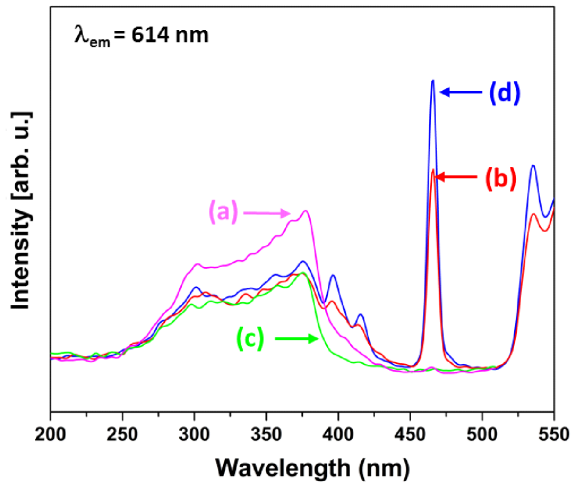


Fig. 5. Excitation spectra of the annealed (a) ZnO and (b)  $\text{Zn}_{0.99}\text{O}:0.01\text{Eu}^{3+}$  powders synthesized at  $150^\circ\text{C}$  and of the annealed (c) ZnO and (d)  $\text{Zn}_{0.99}\text{O}:0.01\text{Eu}^{3+}$  powders synthesized at  $250^\circ\text{C}$ .

$\text{Zn}_{0.99}\text{O}:0.01\text{Eu}^{3+}$  powders synthesized at  $250^\circ\text{C}$  is much stronger than that at  $150^\circ\text{C}$  because of its increased powder size and improved crystallinity. This means that the PL properties of annealed  $\text{Zn}_{0.99}\text{O}:0.01\text{Eu}^{3+}$  powders can be effectively improved by controlling the synthesis temperature.

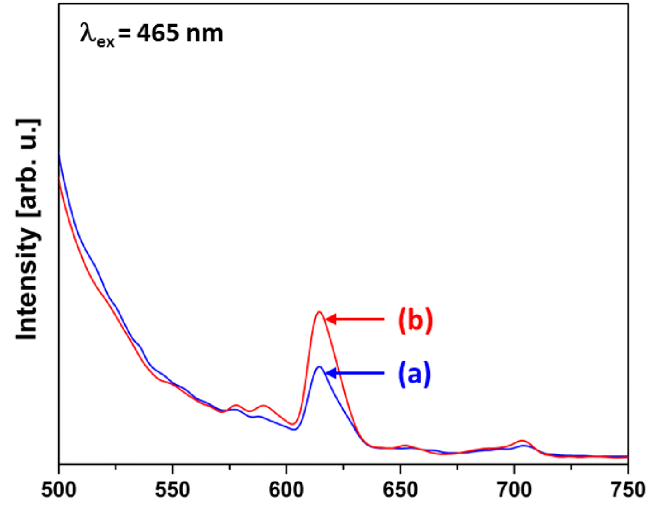


Fig. 6. Emission spectra of the annealed  $\text{Zn}_{0.99}\text{O}:0.01\text{Eu}^{3+}$  powders synthesized at (a)  $150^\circ\text{C}$  and (b)  $250^\circ\text{C}$  upon 465 nm excitation.

#### 4. Conclusions

The hydrothermal temperature affected significantly the size and morphology of the ZnO and  $\text{Zn}_{0.99}\text{O}:0.01\text{Eu}^{3+}$  powders. The ZnO and  $\text{Zn}_{0.99}\text{O}:0.01\text{Eu}^{3+}$  powders synthesized at 150 and  $250^\circ\text{C}$  showed rod- and flower-like morphologies, respectively. The as-synthesized and annealed ZnO and  $\text{Zn}_{0.99}\text{O}:0.01\text{Eu}^{3+}$  powders crystallized in the wurtzite crystal structure and  $P6_3mc$  space group. The crystallite size of as-synthesized ZnO powders increased by annealing and doping the  $\text{Eu}^{3+}$ . The XPS spectra of as-synthesized  $\text{Zn}_{0.99}\text{O}:0.01\text{Eu}^{3+}$  powders exhibited the presence of the constituent elements, Zn, Eu, and O. Sharp excitation peaks were observed at 396, 416, 465, and 536 nm, which correspond to the  ${}^7F_0 \rightarrow {}^5L_6$ ,  ${}^7F_0 \rightarrow {}^5D_3$ ,  ${}^7F_0 \rightarrow {}^5D_2$ , and  ${}^7F_0 \rightarrow {}^5D_1$  transitions of  $\text{Eu}^{3+}$  ions, respectively. Strong emission peaks were detected at 580, 592, 612, 652, and 708 nm, which originate from the  ${}^5D_0 \rightarrow {}^7F_J$  ( $J = 0-4$ ) transitions of  $\text{Eu}^{3+}$  ions. The annealed  $\text{Zn}_{0.99}\text{O}:0.01\text{Eu}^{3+}$  powders synthesized at  $250^\circ\text{C}$  showed much stronger emission intensity than that at  $150^\circ\text{C}$  because of its increased powder size and improved crystallinity.

#### Acknowledgments

We also acknowledge the financial support by the Human Resources Development of the Korea Institute of Energy Technology Evaluation and Planning (KETEP)

grant funded by the Korea government Ministry of Trade, Industry and Energy (No. 20164030201340).

### References

- [1] L. Bian, F. Du, S. Yang, Q. Ren, Q.L. Liu, *J. Lumin.* **137**, 168 (2013).
- [2] H. Chen, C. Li, Y. Hua, L. Yu, Q. Jiang, D. Deng, S. Zhao, H. Ma, S. Xu, *Ceram. Int.* **40**, 1979 (2014).
- [3] W. Chen, *J. Alloys Comp.* **550**, 320 (2013).
- [4] Z. Lu, L. Zhang, L. Wang, Q. Zhang, *J. Nanomater.* **2012**, 1 (2012).
- [5] X. Zhang, B. Liu, W. Yang, X. Jiang, *Prog. Nat. Sci. Mater. Int.* **26**, 312 (2016).
- [6] R. Yu, H.M. Noh, B.K. Moon, B.C. Choi, J.H. Jeong, K. Jang, S.S. Yi, J.K. Jang, *J. Alloys Comp.* **576**, 236 (2013).
- [7] B.V. Rao, M. Jayasimhadri, J. Junho, J. Kiwan, L. Ho Sueb, Y. Soung-Soo, J. Jung-Hyun, *J. Phys. D* **43**, 395103 (2010).
- [8] A. Franco Jr, H.V.S. Pessoni, *Physica B* **476**, 12 (2015).
- [9] S. Kanchana, M.J. Chithra, S. Ernest, K. Pushpanathan, *J. Lumin.* **176**, 6 (2016).
- [10] M. Chandrasekhar, H. Nagabhushana, S.C. Sharma, K.H. Sudheer Kumar, N. Dhananjaya, D.V. Sunitha, C. Shivakumara, B.M. Nagabhushana, *J. Alloys Comp.* **584**, 417 (2014).
- [11] Y.-P. Du, Y.-W. Zhang, L.-D. Sun, C.-H. Yan, *J. Phys. Chem. C* **112**, 12234 (2008).
- [12] L. Yang, Z. Jiang, J. Dong, A. Pan, X. Zhuang, *Mater. Lett.* **129**, 65 (2014).
- [13] L.F. Koao, F.B. Dejene, R.E. Kroon, H.C. Swart, *J. Lumin.* **147**, 85 (2014).
- [14] B. Tang, G. Wang, L. Zhuo, J. Ge, L. Cui, *Inorg. Chem.* **45**, 5196 (2006).
- [15] G. Li, L. Li, M. Li, W. Bao, Y. Song, S. Gan, H. Zou, X. Xu, *J. Alloys Comp.* **550**, 1 (2013).
- [16] S. Bai, S. Chen, Y. Zhao, T. Guo, R. Luo, D. Li, A. Chen, *J. Mater. Chem. A* **2**, 16697 (2014).
- [17] Y.-P. Du, Y.-W. Zhang, L.-D. Sun, C.-H. Yan, *J. Phys. Chem. C* **112**, 12234 (2008).
- [18] J. Petersen, C. Brimont, M. Gallart, G. Schmerber, P. Gilliot, C. Ulhaq-Bouillet, J.-L. Rehspringer, S. Colis, C. Becker, A. Slaoui, A. Dinia, *J. Appl. Phys.* **107**, 123522 (2010).
- [19] A.S. Kamble, B.B. Sinha, K. Chung, M.G. Gil, V. Buringale, C.-J. Park, J.H. Kim, P.S. Patil, *Electrochim. Acta* **149**, 386 (2014).
- [20] J. Huang, S. Liu, B. Gao, T. Jiang, Y. Zhao, S. Liu, L. Kuang, X. Xu, *J. Nanosci. Nanotechnol.* **14**, 3052 (2014).
- [21] Y. Liu, W. Luo, R. Li, X. Chen, *Opt. Lett.* **32**, 566 (2007).
- [22] T.-H. Fang, Y.-S. Chang, L.-W. Ji, S.D. Prior, W. Water, K.-J. Chen, C.-F. Fang, C.-N. Fang, S.-T. Shen, *J. Phys. Chem. Solids* **70**, 1015 (2009).
- [23] Y.Q. Chen, J. Jiang, Z.Y. He, Y. Su, D. Cai, L. Chen, *Mater. Lett.* **59**, 3280 (2005).
- [24] I.P. Sahu, D.P. Bisen, N. Brahme, R.K. Tamrakar, G. Banjare, P. Dewangan, *J. Mater. Sci. Mater. Electron.* **27**, 1 (2016).
- [25] M. Chandrasekhar, H. Nagabhushana, Y.S. Vidya, K.S. Anantharaju, S.C. Sharma, H.B. Premkumar, S.C. Prashantha, B.D. Prasad, C. Shivakumara, R. Saraf, H.P. Nagaswarupa, *J. Mol. Catal. A* **409**, 26 (2015).